Journal of Electronic Materials (2026) 55:2219–2228
https://doi.org/10.1007/s11664-025-12496-0

ORIGINAL RESEARCH ARTICLE

Chirality-Dependent Cutoff Frequency and *I–V* Characteristics in Graphene Nanoribbon-Based FETs

Banafsheh Alizadeh Arashloo[1]

Received: 1 September 2025 / Accepted: 13 October 2025 / Published online: 27 December 2025

Abstract

Graphene-based transistors are suitable candidates for overcoming the scaling problems of Si-based devices in radio frequency (RF) applications and nanoscale devices. The graphene nanoribbon (GNR) is a one-dimensional member of graphene-based materials which possesses the superior properties of graphene. The crucial demands in device technology, particularly the need for high-speed performance, have led to the selection of GNR field-effect transistor (FETs) as a solution for addressing and overcoming scaling issues. In the present work, the cutoff frequency, time delay, and *I–V* characteristics of GNR-based FETs are investigated as indispensable parameters for transistor speed, and their impact on the design and implementation of GNR-based FETs is explored. GNRs are employed in the channel region of metal–oxide–semiconductor FETs to numerically and analytically investigate the cutoff frequency and time delay, which are critical for high-speed switching performance. The Y-parameter in unity current gain magnitude (0 dB) within the quasi-static approximation is used in the model. Results show that increased delay time is associated with reduced channel conductance and corresponding decrease in cutoff frequency. Conversely, high-frequency operation is achieved at low drain–source voltage with small delay times and enhanced channel conductance. In addition, the small output conductance enables Early voltage reduction, leading to a significantly improved voltage gain as confirmed by the *I–V* characteristics. The proposed model demonstrates good agreement with conventional device behavior, validating its accuracy and applicability. Additionally, a comparison of the armchair GNR (AGNR) and zigzag GNR (ZGNR) channels shows that ZGNRs maintain stable current and cutoff frequency with minimal chirality and length effects, while AGNRs exhibit chirality-dependent reductions in current and increased cutoff frequency. This highlights ZGNRs' stability and AGNRs' sensitivity for future nanoscale device applications.

Keywords Graphene nanoribbon FET · cutoff frequency · delay time · (*I–V*) characteristic · armchair and zigzag GNR

Introduction

In recent decades, the perfect potential and performance of graphene-based field-effect transistors (GFET) in radio frequency (RF) applications has attracted considerable research attention; however, poor voltage gain is a limiting factor in their utilization in RF electronics.[1] The transconductance g_m and the output conductance g_d (the inverse of the transistor's output resistance) define the voltage gain as g_m/g_d. The transconductance in graphene is small (up to 5.9 mS/μm), and the weak current saturation obtains comparable g_d and insignificant voltage gain. Therefore, it has been a major challenge in GFETs to increase gain in constant g_m by decreasing g_d.[2] The small bandgap in graphene results in reduced output conductance and solves the voltage gain challenges.[2,3] Moreover, a decrease in the output conductance also improves the thermal stability of the graphene-based RF circuit.[4] Bilayer graphene GFETs have been reported in order to obtain GFETs with a large gain in voltage A_V.[2] Additionally, for investigation of RF applications, key parameters or figures of merit (FOMs) include the transconductance (g_m), intrinsic capacitance (C_{gs} and C_{gd}), and cutoff frequency (fT), in addition to large-signal FOMs such as the power gain (GP), power-added efficiency, and output power (P_{OUT}).[5] Recently, a new performance benchmark was reported for flexible carbon nanotube (CNT)-based RF metal–oxide–semiconductor field-effect transistors (MOSFETs), achieving current gain and power gain cutoff frequencies both exceeding 100 GHz, demonstrating their

✉ Banafsheh Alizadeh Arashloo
balizadeh@gelisim.edu.tr.com

1 Department of Electrical Engineering, Gelişim University, İstanbul, Turkey

potential for high-performance flexible RF applications.[17] Another study reported MOSFETs based on a range of CNT films exhibiting cutoff frequencies beyond 1 THz for devices with a gate length of 80 nm, while transistors with reduced gate length of 35 nm revealed an extrinsic cutoff frequency of up to 551 GHz in sixth-generation wireless communications applications.[18] Digital and analog applications face continual demand for the development of faster electronic devices. Therefore, researchers have attempted to quantify the working of fast FETs over various FOMs. Unfortunately, a unique FOM for quantifying the speed has not yet been found. The maximum oscillation frequency f_{max} and the cutoff frequency f_T are the main FOMs. These parameters are important factors in the transition of frequency from amplification to diminution.[6] When the drain and gate current become the same or when the current gain is equal to 0 dB, the cutoff or 3 dB frequency f_T is defined.[7–9] In other words, f_{max} is the frequency in the 0 dB power gain.[10] Scaling problems with silicon complementary metal–oxide–semiconductor (CMOS) technology has limited the development of devices such as NMOS and PMOS transistors. Therefore, the poor stability of silicon below 10 nm has led to the search for materials as an alternative to silicon. Graphene and its derivatives are excellent alternative candidates. Graphene FETs have emerged as the next generation of devices due to their superior properties over traditional silicon-based transistors. Advantages include low-cost fabrication and the potential for high-speed and low-power operation, as well as higher electron mobility, higher on/off ratio, and excellent device stability.[11] In the present work, fT is modeled to quantify the speed of nanoscale FETs based on a graphene nanoribbon (GNR) channel with few-nanometer dimensions for digital or analog terahertz (THz) applications and appropriate FOM parameters in radio frequency (RF) applications. Therefore, the linear frequency which is obtained for the Y-parameter when the current gain magnitude drops to unity (0 dB) is modeled. The expression of this intrinsic cutoff frequency within the quasi-static approximation[6] is obtained for the GNRFET by the GNR channel. Finally, a comparative analysis of *I*–*V* characteristics and cutoff frequency in armchair (armchair) (n, n) and zigzag (zigzag) (n, 0) GNR channels reveals distinct chirality-dependent behaviors. Zigzag GNRs (ZGNRs) exhibit stable, nearly constant current with minimal variations, reflecting semiconductor-like behavior, whereas armchair GNRs (AGNRs) show a notable decrease in current and significant fluctuations in cutoff frequency with increasing chirality. These results emphasize the superior stability of ZGNRs and the chirality-sensitive response of AGNRs, highlighting their potential for complementary roles in high-frequency and nanoscale electronic devices and in RF applications.

Model

The intrinsic cutoff frequency is achieved for the common-source structure of the FET as shown in Fig. 1b. In the two-port network model of Fig. 1c, the relationship between the Y-parameter matrix and the voltage phasors $\boldsymbol{V}_{\boldsymbol{m}}(\boldsymbol{\omega})$ and current phasors $\boldsymbol{I}_{\boldsymbol{m}}(\boldsymbol{\omega})$ is expressed as[6]

$$V_m(\omega) \equiv \mathcal{F}\left\{V_m(\omega) - V_m(\omega)\right\}, I_m(\omega) \equiv \mathcal{F}\left\{I_m(\omega) - I_m(\omega)\right\} \tag{1}$$

where $\mathcal{F}\{\dots\}$ is the Fourier transform and ω is the angular frequency.

$$\begin{bmatrix} \boldsymbol{I}_1(\boldsymbol{\omega}) \\ \boldsymbol{I}_2(\boldsymbol{\omega}) \end{bmatrix} = \begin{bmatrix} \boldsymbol{Y}_{11}(\boldsymbol{\omega}) & \boldsymbol{Y}_{12}(\boldsymbol{\omega}) \\ \boldsymbol{Y}_{21}(\boldsymbol{\omega}) & \boldsymbol{Y}_{22}(\boldsymbol{\omega}) \end{bmatrix} \begin{bmatrix} \boldsymbol{V}_1(\boldsymbol{\omega}) \\ \boldsymbol{V}_2(\boldsymbol{\omega}) \end{bmatrix}, \tag{2}$$

where $\boldsymbol{Y}_{\boldsymbol{mn}}(\boldsymbol{\omega})$ yields

$$\boldsymbol{Y}_{\boldsymbol{mn}}(\boldsymbol{\omega}) = \frac{\Delta \boldsymbol{I}_m}{\Delta \boldsymbol{V}_n} + \frac{j\boldsymbol{\omega}}{\Delta \boldsymbol{V}_n} \int_0^{\tau_d} (\boldsymbol{I}_{\boldsymbol{S}\boldsymbol{m}}(\boldsymbol{t}) - \boldsymbol{I}_{\boldsymbol{m}}(\boldsymbol{\tau}_{\boldsymbol{d}}))\boldsymbol{e}^{-j\omega t}\mathbf{d}\boldsymbol{t}. \tag{3}$$

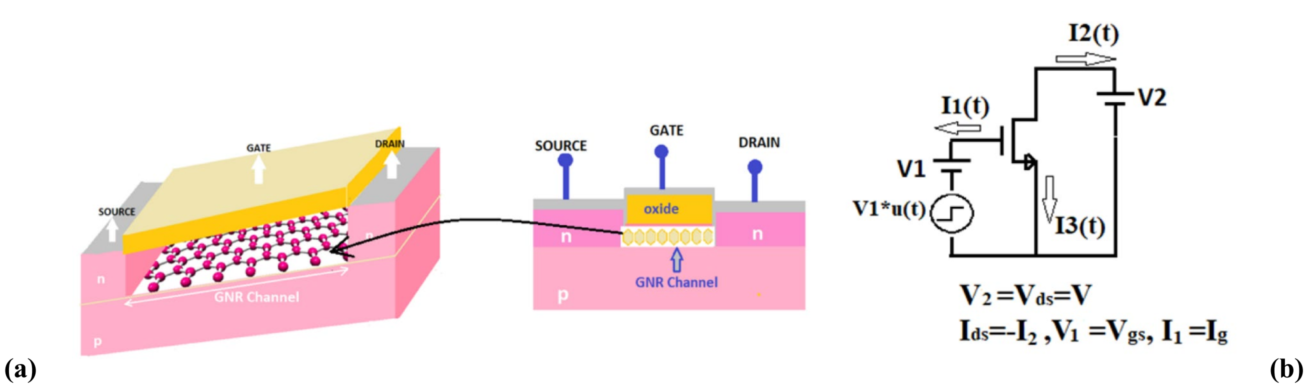

Fig. 1 (a) Schematic of GNRFET transistor by GNR zigzag axis channel. (b) Transistor circuit for cutoff frequency.

According to the cutoff frequency definition, the current gain drops to zero or 0 dB.[6,9] Also,

$$\left|\frac{Y_{21}(\omega)}{Y_{11}(\omega)}\right| \equiv 1 \equiv h_{21}(\omega = 2\pi f_T). \tag{4}$$

The cutoff frequency within the quasi-static approximation ($e^{-j\omega t} = 0$) is found by calculating the term Y_{21} from (3) as

$$Y_{21}(\omega) \equiv \frac{\Delta I_2}{\Delta V_1} \equiv \frac{dI_2}{dV_1} \equiv g_m. \tag{5}$$

The term $Y_{11}(\omega)$ is obtained for the zero-order approximation($e^{-j\omega t} = 1$) from (3) as

$$Y_{11}(\omega) = \frac{\Delta I_1}{\Delta V_1} + \frac{j\omega}{\Delta V_1}\int_0^{\tau_d}(I_1(t) - I_1(\tau_d))dt \cong \frac{j\omega}{\Delta V_1}\Delta Q_1 \cong j\omega C_{gs}. \tag{6}$$

Therefore, the current pulse wide τ_d based on the quasi-static assumption is sufficiently short to neglect any modification factor of the drain current. Thus, the cutoff frequency, as explained, is obtained from (5) and (6) as

$$f_T = \frac{g_m}{2\pi C_{gs}}. \tag{7}$$

During the transient evolution or quasi-static approximation, $\Delta Q1 \approx \Delta Q2$ is assumed, and hence

$$\Delta Q_1 \approx \Delta Q_2 \equiv \int_0^{\tau_d}(I_2(t) - I_2(\tau_d))dt \equiv \Delta I_2.\tau_d. \tag{8}$$

Assuming that $\Delta Q_1 \approx \Delta Q_2 \cong \Delta V_1.C_1$ and from (8), we can obtain[6]

$$g_m \equiv \frac{dI_2}{dV_1} \equiv \frac{\Delta I_2}{\Delta Q_1}\frac{\Delta Q_1}{\Delta V_1} \equiv \frac{C_{gs}}{\tau_d}. \tag{9}$$

Therefore, $f_T = \frac{1}{2\pi\tau_d}$, where the intrinsic delay time is τ_d. This means that the intrinsic delay time is much greater than the time-based or temporal width of the current pulse created by one electron τ_p ($\tau_d > \tau_p$), although in short-channel FET transistors, a time-dependent electric field is generated by moving an electron along the channel without even passing the drain and source contact surfaces and so on ($\tau_d \cong \tau_p$).[7] Consequently, in the present work, the assumption $\tau_d \cong \tau_p$ can be accepted which included nanoscale FET devices based on GNRs with the nanoscale channel.

The model of the conductance using the Landauer formula for the GNR is considered as[12]

$$G = \frac{-q^2}{hL}\left(\sqrt{\frac{3atk_B T}{\beta}}\right)(\Im_{-\frac{1}{2}}(\eta) + \Im_{-\frac{1}{2}}(-\eta)), \tag{10}$$

where k_B is the Boltzmann constant, q is the charge, the carbon–carbon (C–C) bond length is $a_{c-c} = a = 1.42A°$, the tight binding overlap energy of the nearest neighbor is t=2.7ev, T is the local temperature, β is the wave vector,[15] h is the Planck constant, $\Im_i(\eta)$ is the Fermi integral of order i, and η is the normalized energy which is equal to $\eta = \frac{qV}{k_B T}$, where V is the applied voltage between two electrodes.[12] The effective mobility from the Drude model ($\mu_{eff} = \frac{GL}{n_g q}$), $n_g = 7 \times 10^7$,[13] is given by

$$\mu_{eff} = \frac{-q}{n_g h}\left(\sqrt{\frac{3atk_B T}{\beta}}\right)\left(\Im_{-\frac{1}{2}}(\eta) + \Im_{-\frac{1}{2}}(-\eta)\right). \tag{11}$$

In addition, the carrier concentration N in the parabolic band structure of graphene is given by

$$N = \left(\sqrt{\frac{2m^* k_B T}{\pi h^2}}\right)\Im_{-\frac{1}{2}}(\eta), \tag{12}$$

where m^* is the effective mass. The intrinsic delay time or charge carrier delay τ_d is the relaxation time, which is equal to $\tau = \frac{m^*}{2\pi e}\mu$, where e is the electron charge, and from $f_T = \frac{1}{2\pi\tau_d}$ we can obtain the cutoff frequency of the transistor by

$$f_T = \frac{n_g qe}{m^* LG}. \tag{13}$$

Therefore, by replacing the carrier concentration and the conductance model in Eq. 13, we obtain

$$f_T = \frac{ehn_g}{m^* q(\Im_{-\frac{1}{2}}(\eta) + \Im_{-\frac{1}{2}}(-\eta))}\left(\sqrt{\frac{\beta}{3atk_B T}}\right). \tag{14}$$

From Eq. 7, $g_m = 2\pi C_{gs} f_T$ is considered as

$$g_m = \frac{2\pi e\, hn_g C_{gs}}{m^* q\left(\Im_{-\frac{1}{2}}(\eta) + \Im_{-\frac{1}{2}}(-\eta)\right)}\left(\sqrt{\frac{\beta}{3atk_B T}}\right). \tag{15}$$

Also, from Eq. 9, τ_d is obtained as

$$\tau_d \equiv \frac{C_{gs}}{g_m} = \frac{m^* q}{2\pi e\, hn_g}\left(\sqrt{\frac{3atk_B T}{\beta}}\right)\left(\Im_{-\frac{1}{2}}(\eta) + \Im_{-\frac{1}{2}}(-\eta)\right). \tag{16}$$

The amount of charge in the channel depends on the gate–source voltage ($q = C_{gs}V_{gs} = \frac{I}{t}$); therefore, the current density between the drain and source is $J_{sd} = \frac{I}{A} = \frac{\tau_d C_{gs} V_{gs}}{A}$, when the carrier delay time is equal to $t = \tau_d$. By considering Eq. 16, the drain source equation can be obtained as

$$J_{sd} = \frac{\tau_d C_{gs} V_{gs}}{A} = \frac{m^* q C_{gs} V_{gs}}{2A\pi e \, hn_g}\left(\sqrt{\frac{3atk_B T}{\beta}}\right)\left(\mathfrak{F}_{-\frac{1}{2}}(\eta) + \mathfrak{F}_{-\frac{1}{2}}(-\eta)\right). \quad (17)$$

The channel current density is modeled based on the intrinsic parameters of the GNR. As illustrated in Fig. 2a, an increase in the gate–source capacitance enhances the channel current ($(I = J_{sd}/A)$). However, this increase also leads to a reduction in the Early voltage ($V_A \propto g_d$), which consequently increases the current gain while decreasing the output resistance. This trade-off negatively affects the voltage gain in RF applications. To maintain a high voltage gain, a proper balance between the gate–source voltage V_{gs} and the Early voltage must be achieved. As a result, the output resistance increases slightly at lower gate–source voltages. Furthermore, enhancing the gate voltage promotes a higher channel current for a constant gate–source capacitance. At low gate voltages, channel pinch-off occurs, where the drain current approaches zero while the voltage gain reaches its maximum. These findings define the characteristic behavior of high-performance GNRFETs and validate the analytical model proposed in this study.

As is well established, an increase in gate–source capacitance results in a reduction in the cutoff frequency, as indicated by Eq. 7. Correspondingly, Fig. 2c and d demonstrates that a higher gate–source capacitance enhances channel conductance due to an increase in carrier delay (intrinsic time) within the channel. For a constant delay time, the channel conductance is greater at higher gate–source capacitance values than at lower values. This observation underscores the critical role of C_{gs} by extension of the oxide thickness—in determining both the delay time and carrier concentration. Conversely, smaller capacitance values enable higher

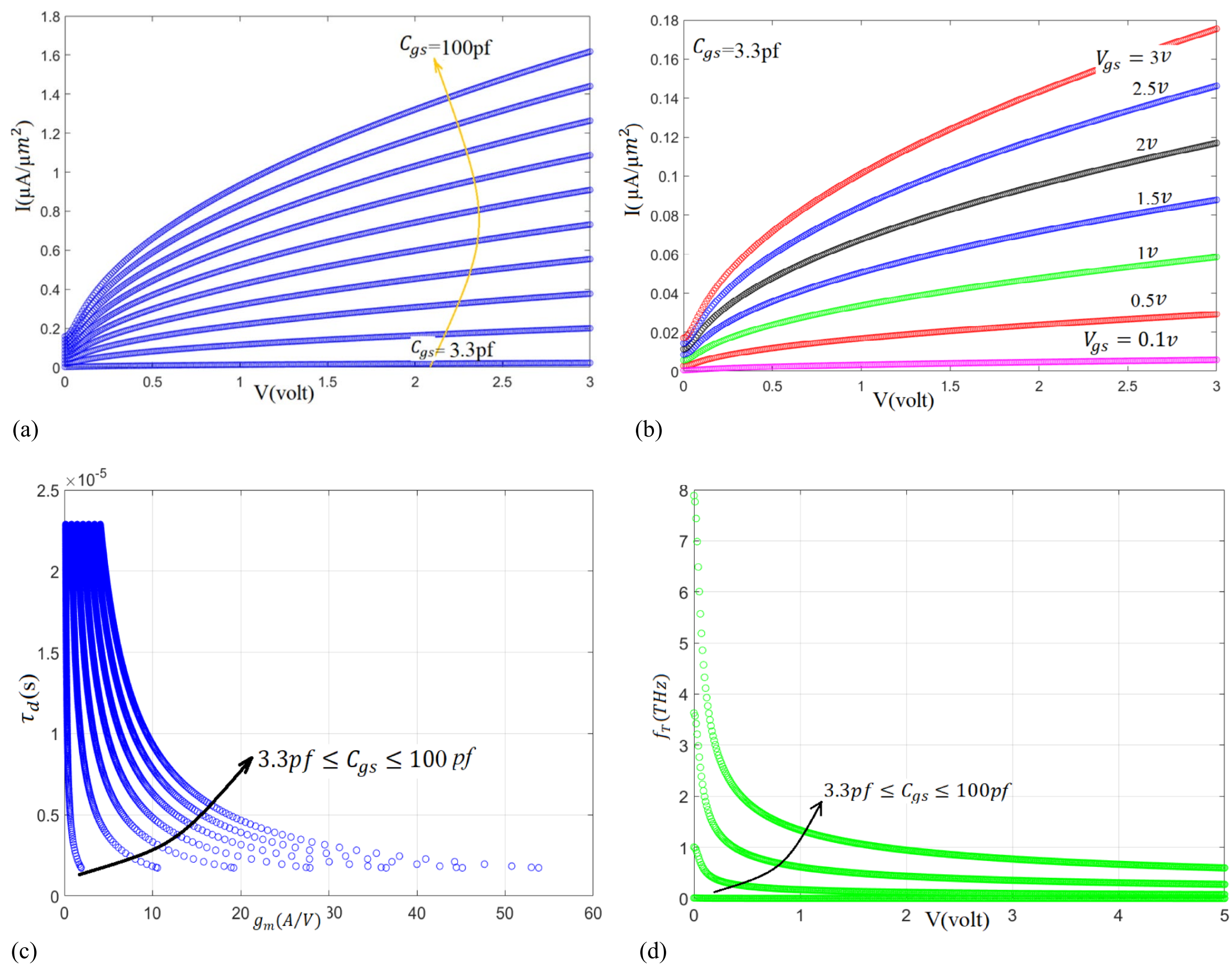

Fig. 2 The variation in the *I–V* characteristic by (a) gate and source capacitor $(3.3pf \le C_{gs} \le 100pf)$ and (b) gate–source voltage $0.1V \le V_{gs} \le 3V$. (c) The variation in delay time by channel conductance and C_{gs}. (d) The variation in cutoff frequency with changes in channel voltage and C_{gs}.

cutoff frequencies and faster GNRFET operation but at the expense of reduced channel conductance and lower voltage gain. Moreover, an increased drain–source bias (V_{ds}) can further degrade the cutoff frequency, particularly in devices with low C_{gs}, emphasizing the importance of balancing capacitance, operating speed, conductivity, and voltage gain in GNRFET design.

The impact of temperature on the cutoff frequency is illustrated in Fig. 3 for the range 25 mev $\leq K_B T \leq$ 50 mev. As observed, the cutoff frequency decreases with increasing temperature, indicating that the carrier delay time becomes longer at higher temperatures. Consequently, elevated temperatures lead to an increase in intrinsic carrier delay, which accounts for the reduction in channel conductance and the corresponding decline in cutoff frequency. Nevertheless, as shown in Fig. 2a, an increase in temperature can also enhance channel conductance despite the reduction in delay time, revealing a complex trade-off among conductance, delay, and cutoff frequency in GNRFET devices.

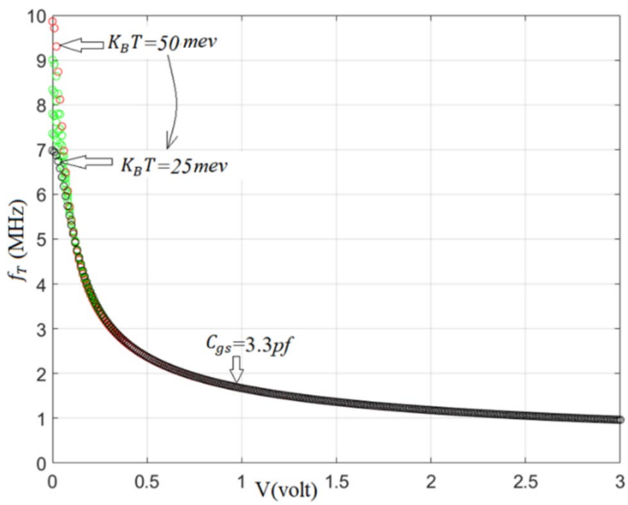

Fig. 3 Variation in cutoff frequency by channel voltage , constant C_{gs}, and temperature change effect by 25mev $\leq K_B T \leq$ 50mev.

A comparison between the proposed analytical model and previously reported simulation results is presented in Fig. 4a. The *I–V* characteristics of the model are plotted for $C_{gs} = 3.3pf$ and $V_{gs} = 0.5$, 1, and 1.5 V, with the source–drain voltage varying from 0 to 2 V for a channel length of 20 nm. Furthermore, Fig. 4b illustrates the comparison between the proposed model and experimental data for $V_{DS} = 0.1V$ and $0.6 \leq V_{gs} \leq 1.4$, demonstrating strong agreement and validating the model's accuracy. Accordingly, the linear frequency model derived from the Y-parameter at unity current gain magnitude (0 dB) within the quasi-static approximation is obtained for the GNRFET based on a GNR channel. As discussed earlier, the cutoff frequency plays a crucial role in high-frequency transistor applications, such as GNRFETs, which are promising candidates for addressing scaling challenges and for use in nanoscale electronic devices.

The chirality number n is an important parameter in choosing the GNR type. There are two types of ribbon, where the edge configuration determines the type of ribbon. As shown in Fig. 5, by considering the c–c atomic band distance equal to a=0.142 nm and for chirality number (n), the channel length (ribbon) for AGNR and ZGNR is equal to $3a(n)$ and $\sqrt{3}a(n)$, respectively. The wave vector β is defined as[15]

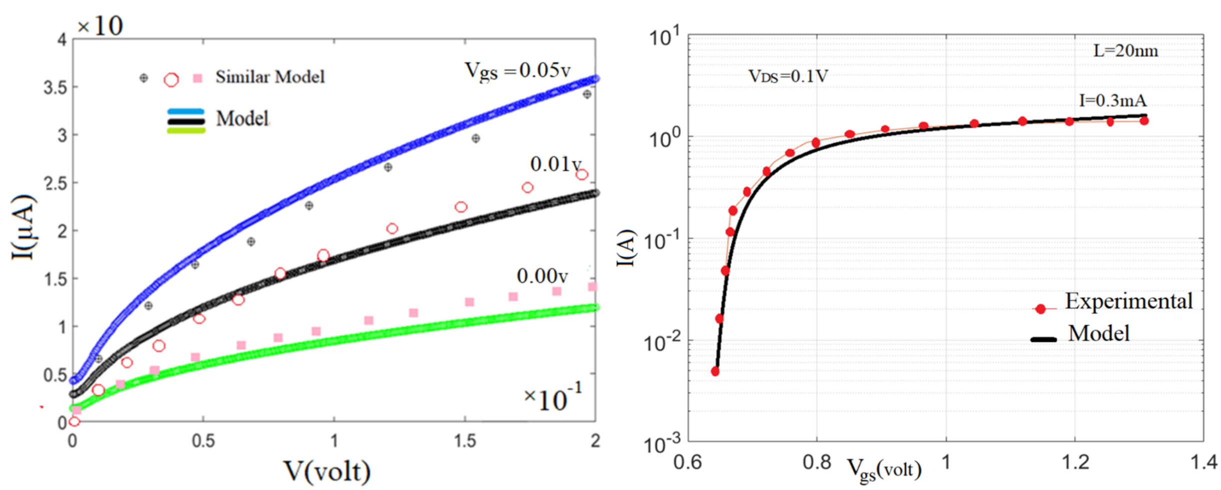

(a) (b)

Fig. 4 A The comparison of model *I–V* characteristics by simulation of a similar work model [6] in the $C_{gs} = 3.3pf$ and for $V_{gs} = 0.5,1, 1.5V$ in the source and drain voltage variation between 0 and 2 V in the 20 nm channel length. (b) Comparison of model ($I–V_{gs}$) characteristics by experimental device in 20 nm.[14]

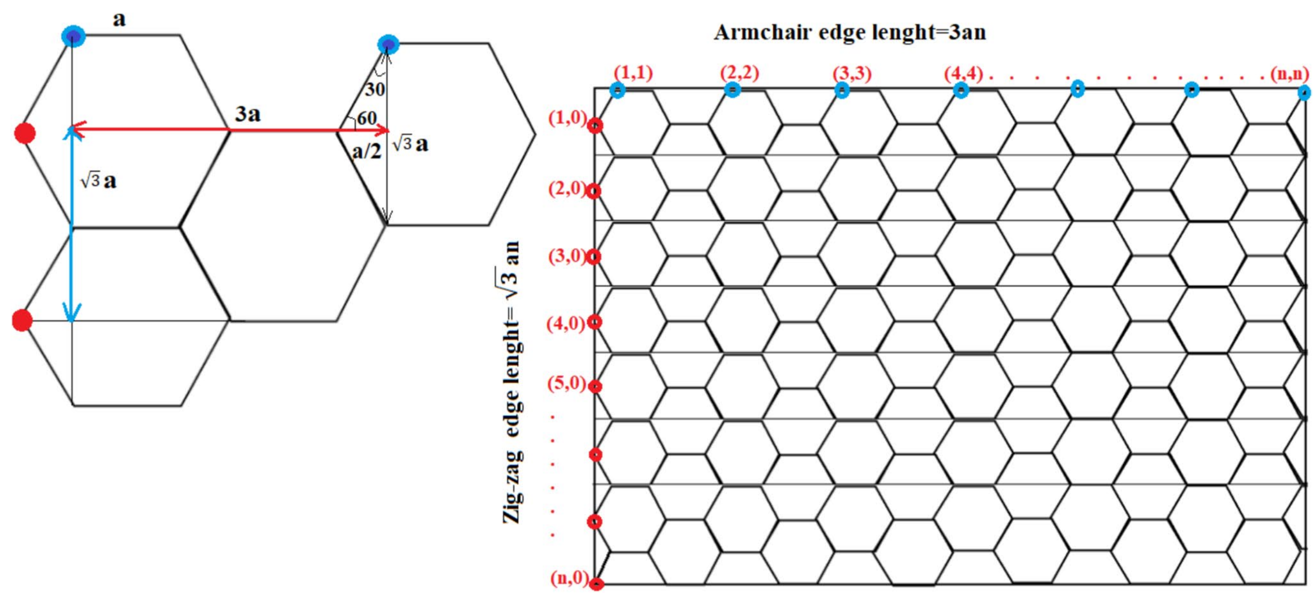

Fig. 5 The transistor channel based on the edge configuration [armchair (n, n) or zigzag (n, 0)]. By considering the c-c atomic distance equal to $a = 0.142$ nm and for chirality number (n), the channel length (ribbon) for AGNR and ZGNR is equal to $3an$ and $\sqrt{3}an$, respectively.

$$\beta = \frac{2\pi}{a\sqrt{3}}\left(\frac{p}{n+1} - \frac{2}{3}\right), \quad (18)$$

where n is the chirality number and $p = 1,2,3,\ldots$ p is an integer;$n = 3p$ is for metallic armchair GNR and $n = 3p + 1$ and $3p + 2$ for semiconductor armchair GNR.[16] By substituting Eq. 18 in Eqs. 17 and 14, the chirality number effect is investigated. The *I–V* characteristics and cutoff frequency as a function of voltage for AGNRs with chirality index $n = (p = 1,2,3,\ldots)$, under a voltage range of 0–3 V, are shown in Fig. 6a and b. As can be seen, increasing the chirality number leads to a decrease in current, while the cutoff frequency increases. This indicates that with increasing channel length, both the cutoff frequency and bandwidth increase. Such behavior occurs when the channel exhibits metallic properties, although materials exhibiting metallic behavior are probably not suitable for channel applications. Similarly, Fig. 7a and b shows the *I–V* characteristics and

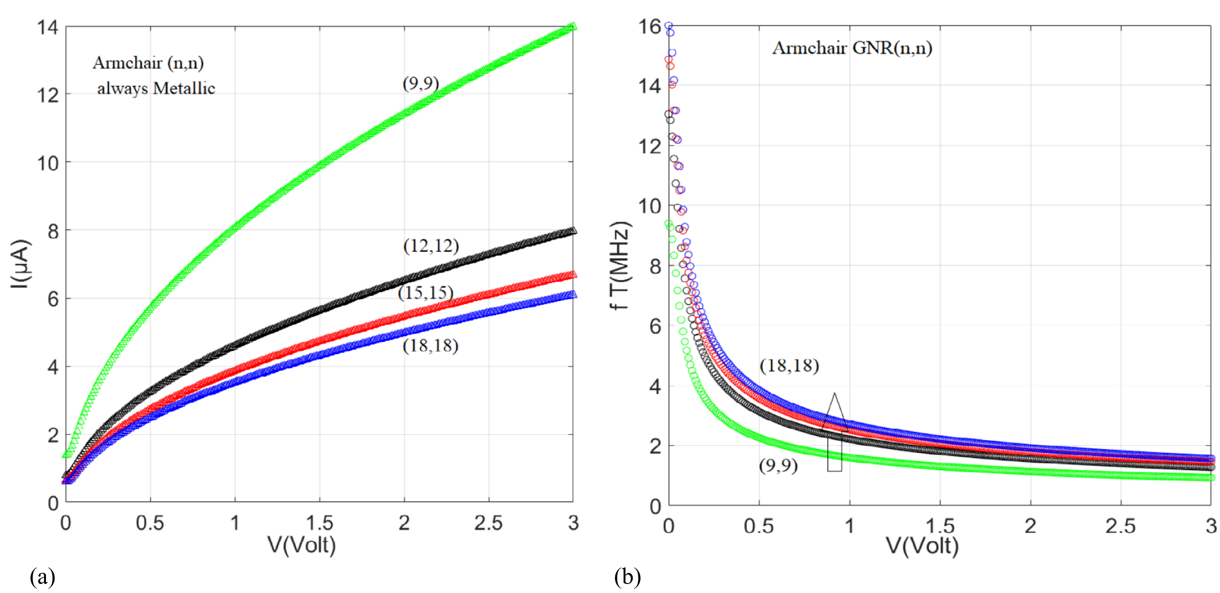

Fig. 6 (a) The *I–V* characteristic and (b) cutoff frequency by voltage, plotted for AGNR by $n = 3p$ ($p = 1,2,3,\ldots$) and voltage variation in the range of (0–3 V).($C_{gs} = 3.3pf$ and $V_{gs} = 1$ V).

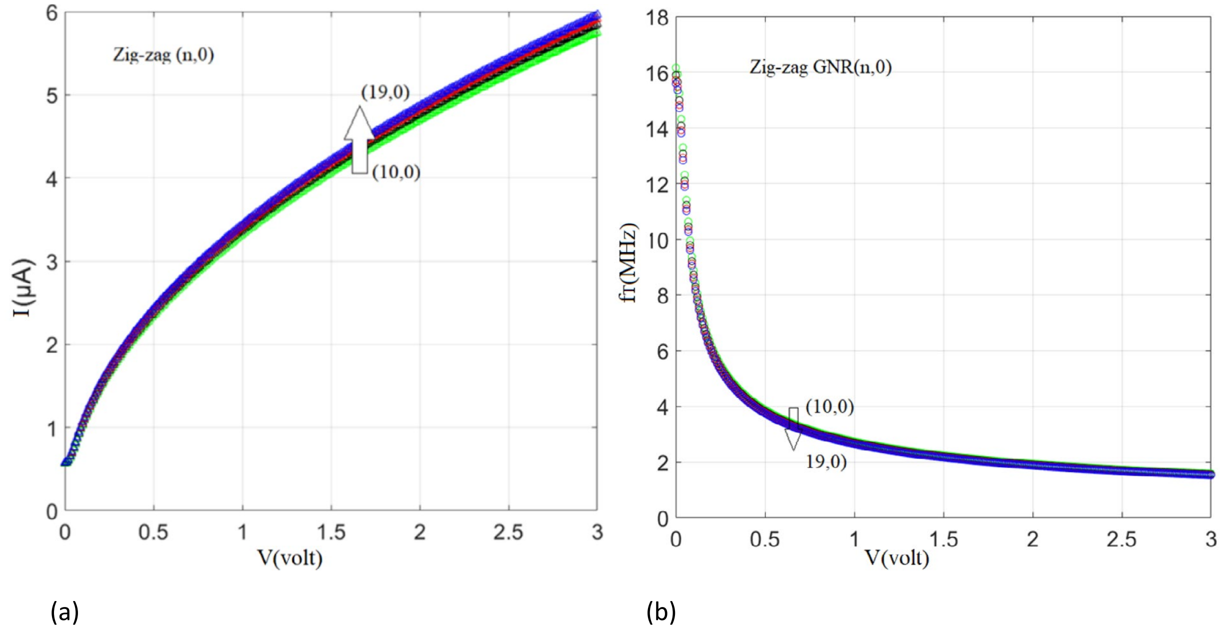

Fig. 7 (a) The *I–V* characteristic and (b) cutoff frequency by voltage, plotted for ZGNR by $n=3p+1$ ($p=1,2,3,..$) and voltage variation in the range of (0–3 V). (C_{gs} = 3.3*pf* and V_{gs} = 1 V).

cutoff frequency for ZGNRs with $n=3p+1$ ($p=1,2,3,...$) in the same voltage range (0–3 V). In this case, the current remains nearly constant, with negligible variations, as the chirality increases. For $n=3p+1$, AGNRs behave as semiconductors, showing more variation than ZGNRs. Consequently, the variation in current and cutoff frequency for ZGNRs are negligible and opposite to the trends observed in AGNRs.

A comparison of the AGNR and ZGNR in the same chirality number is plotted in Fig. 8. In Fig. 8a and b, a comparison of the *I–V* characteristics for $n=17$ and $n=10$ shows that the variation in the zigzag is negligible and can be ignored, while in the AGNR, an increase in the chirality number leads to a decrease in current greater than that in the ZGNR. Figure 8c and d show the cutoff curves versus the voltage variation in the range of (0–3 V), where the variation in the cutoff in the AGNR is greater than ZGNR with the decrease in chiralty, whereas the cutoff frequency is increased with the increase in chirality, as plotted in Fig. 8.

In the final step, the *I–V* characteristics and cutoff frequency as a function of voltage are analyzed. For ZGNR with $n=3p+1$ ($p=1,2, 3,\dots$) in the range of 0–3 V (Fig. 8a and b), the current remains nearly constant, with negligible variation, maintaining consistent metallic behavior. For $n=3p+1$, AGNRs exhibit semiconductor-like behavior, with smaller variations than ZGNRs because of edge-dependent properties. Thus, changes in the current and cutoff frequency for ZGNR are negligible and opposite to AGNR. A comparison between AGNR and ZGNR (Fig. 8) shows that, for $n=17$ and $n=10$, ZGNR maintains stable current while AGNR shows a clear decrease as chirality increases. Moreover, Fig. 8c and d illustrates that AGNR exhibits a larger variation in cutoff frequency, which increases with chirality number, unlike ZGNR.

In this work, an analytical investigation of GNRFETs is presented, focusing on the modeling of delay time, cutoff frequency, and *I–V* characteristics under varying bias and capacitance conditions. The findings indicate that the intrinsic delay is strongly dependent on the channel conductance, while a reduction in output conductance and an increase in Early voltage enhance the RF voltage gain. The proposed analytical models are validated through numerical simulations, demonstrating strong agreement with experimental data. Moreover, the comparative analysis reveals that ZGNR-based devices exhibit stable current and cutoff frequency characteristics, with minimal sensitivity to chirality, whereas AGNR-based devices show pronounced chirality-dependent variations. These results highlight the superior stability of ZGNRs due to their inherently metallic nature and the enhanced frequency sensitivity of AGNRs, making them promising candidates for nanoscale high-frequency electronic applications.

A comparison between AGNR and ZGNR structures with identical channel lengths is presented in Fig. 9a, corresponding to $n=17$ and $n=9$ for $L=4$ nm, respectively. Similarly, Fig. 9b illustrates the comparison for $n=21$ and $n=41$ at $L=10$ nm. The channel lengths were determined based on Fig. 5 and the established relationship between the chirality index and channel length. As depicted in the figures, increasing the channel length results in a

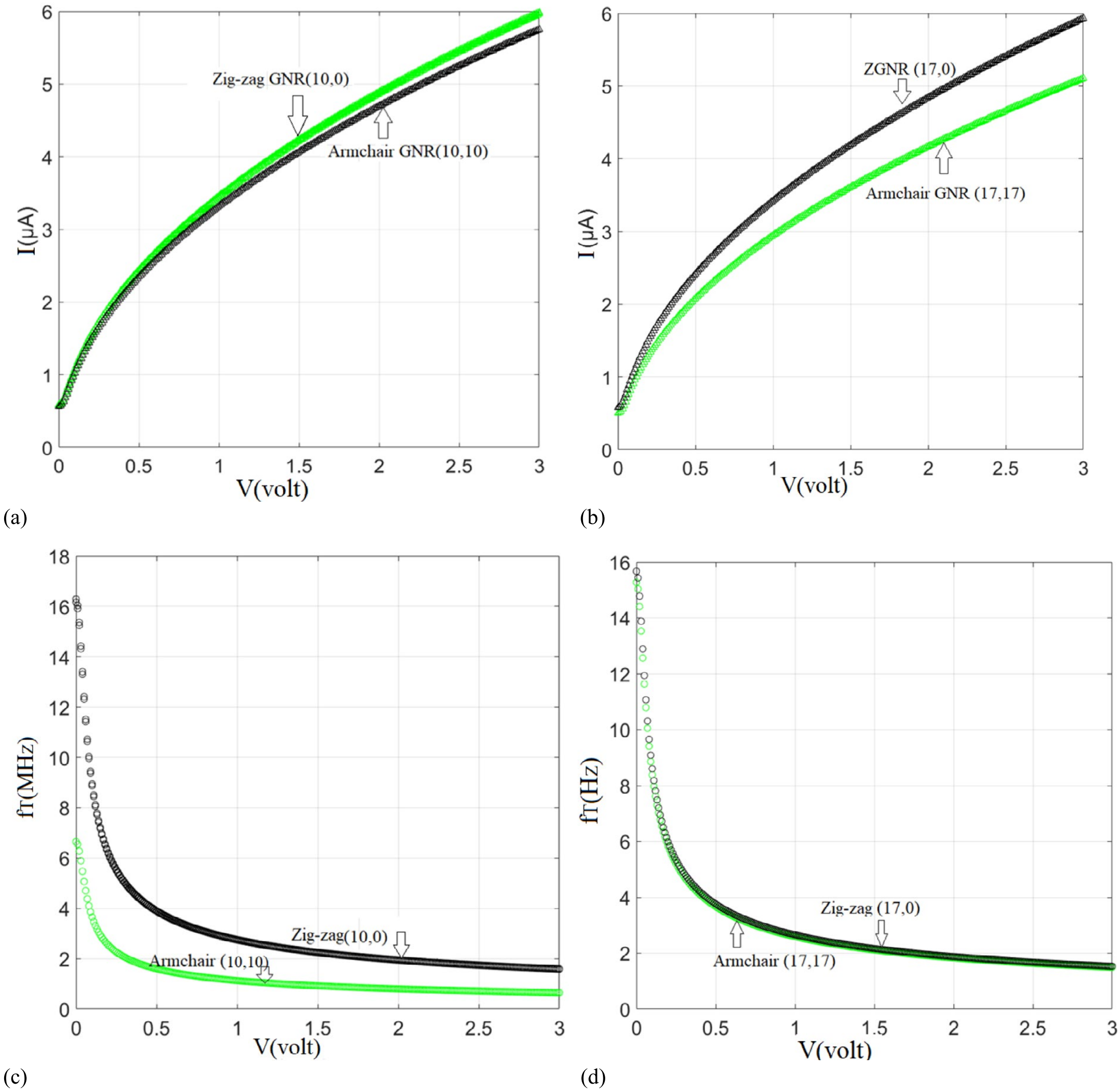

Fig. 8 Comparison between AGNR and ZGNR structures with identical chirality numbers. (a, b) The comparison for $n=17$and $n=10$ illustrates that the variation in current for ZGNR is negligible, whereas an increase in the chirality number results in a more pronounced current reduction in AGNR. (c, d) The cutoff frequency as a function of applied voltage (0–3 V) shows that the variation in the cutoff behavior is more significant in AGNR than in ZGNR. Furthermore, the cutoff frequency in AGNR increases with the chirality number, indicating its stronger dependence on the edge configuration.

noticeable reduction in current for AGNR, whereas the variation for ZGNR remains relatively minor. Comparable behavior can also be observed when analyzing the influence of chirality variation in Fig. 8. Overall, Fig. 9 indicates that the increase in channel length leads to a reduction in the *I–V* characteristic variations of both AGNR and ZGNR, primarily due to the diminishing contribution of quantum confinement effects.

Recently, increasing attention has been devoted to FET transistors that utilize one-dimensional carbon-based channels such as GNRs, graphene nanoscrolls, and related nanostructures. In this work, an analytical investigation of the cutoff frequency in GNR-based FETs is presented. GNRFETs are proposed as promising candidates for RF and high-speed applications, addressing scaling limitations through the evaluation of key FOMs, including delay time, channel conductance, output conductance, and Early voltage. Analytical models are developed for delay time, cutoff frequency, and *I–V* characteristics under varying gate–source voltages and capacitance conditions. The results show that

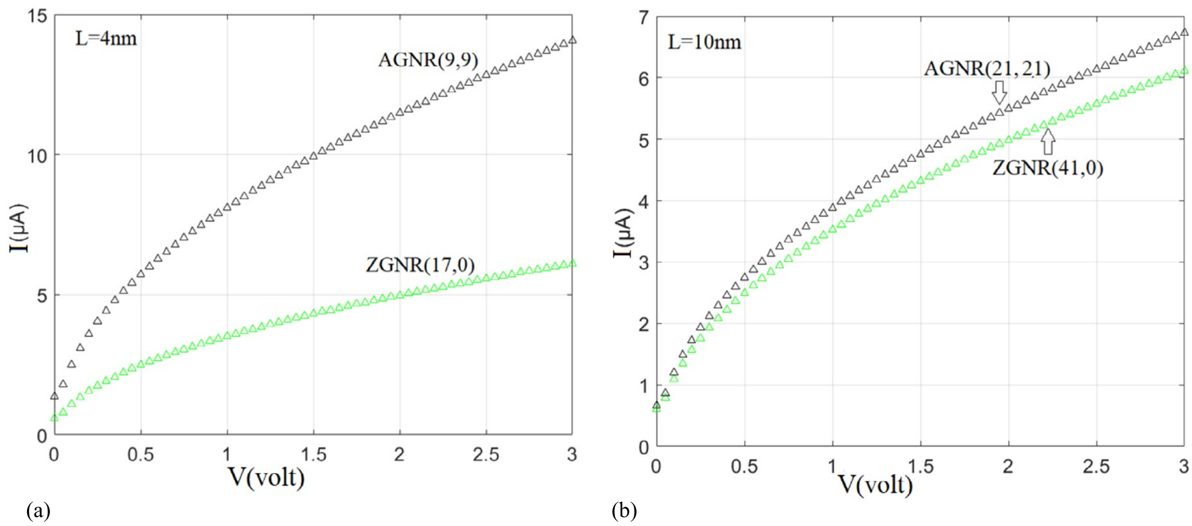

Fig. 9 Comparison of the AGNR and ZGNR of the same length. (a) Comparison of AGNR and ZGNR in $n=17$ and 9, respectively, for $L=4$ nm. (b) Comparison of AGNR and ZGNR in $n=21$ and 41, respectively, for $L=10$nm, which is obtained by Fig. 5.

a large intrinsic delay is directly linked to reduced channel conductance, which limits switching speed, while a decrease in output conductance associated with a lower Early voltage enhances the voltage gain in RF applications. The *I–V* characteristics further confirm that low Early voltage occurs at small gate–source voltages, whereas higher supply voltages result in reduced output conductance and improved voltage gain. Numerical simulations demonstrate strong agreement with experimental data, validating the accuracy and applicability of the proposed model. Additionally, a comparison of *I–V* characteristics and cutoff frequency with respect to chirality number and length is carried out for AGNR and ZGNR channels. In ZGNRs, the current remains nearly constant, with negligible variation, indicating metallic-like behavior with much smaller fluctuations than AGNRs. Consequently, changes in current and cutoff frequency for ZGNRs are minimal and opposite to those observed in AGNRs. In contrast, AGNRs display a significant reduction in current as chirality increases, along with larger variations in cutoff frequency, which increase with chirality number. These findings highlight the superior stability of ZGNRs and the chirality-dependent sensitivity of AGNRs, underscoring their distinct roles in future high-frequency and nanoscale device applications.

Author Contributions The study was conceived and modeled by Dr. Banafsheh Alizadeh Arashloo.

References

1. N. Petrone, I. Meric, T. Chari, K.L. Shepard, and J. Hone, Graphene field-effect transistors for radio-frequency flexible electronics. *IEEE J. Electron Devices Soc.* 3, 44 (2015).
2. B.N. Szafranek, G. Fiori, D. Schall, D. Neumaier, and H. Kurz, Current saturation and voltage gain in bilayer graphene field effect transistors. *Nano Lett.* 12(3), 1324 (2012).
3. S.M. Song et al., Improved drain current saturation and voltage gain in graphene–on–silicon field effect transistors. *Sci. Rep.* 6(1), 25392 (2016).
4. S. Song, J.H. Bong, W. Hwang, B. Wansik, and C.B. Hwang, Gate capacitance modeling and width-dependent performance of graphene nanoribbon transistors. *Microelectron. Eng. Sci. Rep.* 112, 220 (2013).
5. N. Yadava, and R. Chauhan, Evaluation of the RF performance of the β-Ga2O3 negative-capacitance field-effect transistor. *J. Comput. Electron.* 19(2), 603 (2020).
6. Z. Zhan, E. Colomes, and X. Oriols, Limitations of the intrinsic cutoff frequency to correctly quantify the speed of nanoscale transistors. *IEEE Trans. Electron Devices* 64(6), 2617 (2017).
7. L.M. Valdez-Sandoval, E. Ramirez-Garcia, S. Park, D. Akinwande, D. Jimenez, and A. Pacheco-Sanchez, A small-signal description of black-phosphorus transistor technologies for high-frequency applications. *IEEE Microw. Wirel. Components Lett.* 31(9), 1055 (2021).
8. S.E. Laux, Techniques for Small-Signal Analysis of Semiconductor Devices. *IEEE Trans. Comput. Aided Des. Integr. Circuits Syst.* 4(4), 472 (1985).
9. L. Wang, L. Li, N. Lu, Z. Ji, W. Wang, Z. Zong, G. Xu, and M. Liu, An improved cut-off frequency model with a modified small-signal equivalent circuit in graphene field-effect transistors. *IEEE Electron Device Lett.* 36, 1351 (2015).
10. F. Schwierz, Graphene transistors. *Nat. Nanotechnol.* 5(7), 487 (2010).
11. A. Singh, P. Shankar, R.K. Baghel, S. Tirkey, A review on graphene transistors, in *2023 IEEE International Students' Conference on Electrical, Electronics and Computer Science (SCEECS)*, pp. 1–6

12. M.T. Ahmadi, B.A. Arashloo, and T.K. Nguyen, Analytical modeling of graphene oxide based memristor. *Ain Shams Eng. J.* 12(2), 1741 (2021).
13. X. Wang, Y. Ouyang, L. Jiao, H. Wang, L. Xie, J. Wu, J. Guo, and H. Dai, Graphene nanoribbons with smooth edges behave as quantum wires. *Nat. Nanotechnol.* 6(9), 563 (2011).
14. X. Wang, Y. Ouyang, L. Jiao, H. Wang, L. Xie, J. Wu, J. Guo, and H. Dai, Investigation and design of ion-implanted MOSFET based on (18 nm) channel length. *TELKOMNIKA Indones. J. Electr. Eng.* 18, 2635 (2020).
15. Y.W. Son, M.L. Cohen, and S.G. Louie, Energy gaps in graphene nanoribbons. *Phys. Rev. Lett.* 97(21), 216803 (2006).
16. G.W. Hanson, *Fundamentals of Nanoelectronics*. Prentice Hall, p. 385 (2008).
17. F. Xia, T. Xia, H. Su, L. Gan, Q. Hu, W. Wang, R. Huang, T. Bai, Y. Chen, C. Ma, G. Long, S.X. Wang, *Flexible radio-frequency transistors exceeding 100 GHz,* physics.app-ph, https://arxiv.org/abs/2502.02485 (2025).
18. J. Zhou, Z. Pan, L. Ding, L. Xu, X. Cheng, H. Li, F. Yao, C. Jin, M. Zhu, L. Liu, and H. Shi, Terahertz metal–oxide–semiconductor transistors based on aligned carbon nanotube arrays. *Nat. Electron.* (2025). https://doi.org/10.1038/s41928-025-01463-6.